Chapter –2

Literature Review

2.1 Tropospheric biennial oscillation /Quasi -biennial oscillation

A dominant natural oscillation present in the equatorial lower stratosphere is the QBO in zonal wind. The driving force for the QBO is the vertical transfer of momentum from the troposphere to stratosphere by Kelvin and Rossby-Gravity waves. This oscillation is considered as the instability of the mean zonal flow resulting from equatorial wave-mean flow interaction (Holton and Lindzen, 1972; Plumb and Mc Ewan, 1978). One of the challenging problems is the vertical coupling of the QBO in the middle atmosphere and its influence on the tropospheric weather systems etc. Recently Baldwin et al., (2001) reviewed all aspects of QBO including its possible association with tropospheric weather systems. SPARC has taken initiatives to study the QBO and its possible role in coupling stratosphere and troposphere.

Holton and Tan (1980, 1982) showed that the equatorial QBO is found to influence the high latitude stratospheric circulation features like the amplitude of planetary waves, strength of polar jet stream/polar vortex during winter. They found that the polar night jet is stronger (weaker) than normal during the westerly (easterly) phase of the QBO at 50 hPa. It appears that this relationship is influenced by the 11 year solar cycle also (Labitzke and Van Loon, 1988). Baldwin (2000) reported that the phase and strength of the AO or annular mode especially in the stratosphere, are influenced by QBO. The AO tends to be in its negative phase (weak polar vortex) when the QBO is easterly. He suggested that the high latitude stratosphere – troposphere coupling through AO appears to communicate some effect from the QBO to the earth's surface. Gong et al., (2001) found a significant out-of-phase relationship between the AO and East-Asian winter monsoon. Their study revealed that the AO influences the East Asian

winter monsoon through the impact on the Siberian high. Above the lower stratosphere, QBO is found to influence the descending westerly phase of the semi-annual oscillation in the stratopause region (Dunkerton and Delisi, 1997). The QBO tend to affect the vertically propagating waves and causes a strong QBO while these waves reach the mesopause region.

Mukherjee et al., (1985), Bhalme et al., (1987), Mohanakumar (1996) showed evidences for a link between the Indian monsoon activity and the stratospheric wind. A dominant QBO spectral peak in Indian summer monsoon rainfall and the number of monsoon depressions was also reported (Bhalme and Jadhav, 1984). According to Bhalme et al., (1987), the Indian monsoon rainfall tending to be less (more) than normal during easterly (westerly) phase of the QBO at 10 hPa. He also pointed that large-scale floods never occurred during easterly phase and drought almost never during westerly phase. Gray (1984) identified an association between QBO phase and seasonal incidence of Atlantic tropical cyclones. It is unclear how the Indian monsoon activity or Atlantic cyclone incidence have been affected by the phase of the QBO at 10 hPa or 50 hPa (which propagates downward at a speed of 1km/month) just few months prior to their occurrence.

All these relationships are suggestive and based on statistical relationships. Gray (1992) hypothesized a mechanism where by the QBO of zonal winds alters the distribution of intense deep convective activity throughout the tropical west Pacific. He suggested that in conjunction with the annual cycle and the build up of heat in the Pacific warm pool, the QBO linked variations of deep convection cause variations in the central Pacific trade winds and Walker circulation while in turn govern the occurrence of

ENSO events in the tropical Pacific. Recently, the possibility of a QBO driven monsoon variability was investigated in a number of general circulation model experiments by Giorgetta et al., (1999). These experiments showed that the boreal summer monsoon is significantly influenced by the QBO. They also showed that the QBO influence the austral summer monsoon but the precipitation does not change significantly. QBO seemed to modulate dynamical quantities like temperature, wind, potential vorticity (Baldwin and Dunkerton, 1998; Randell et al., 1997), ozone (Bowman, 1989, Tung and Yang, 1994), and aerosol (Hitchman et al., 1994). QBO influences the properties of the ionosphere also (Chen, 1992).

Several studies have suggested the presence of QBO like biennial oscillation in tropical atmosphere (Angell and Korshover, 1974, 1975; Ebdon, 1975; Terray, 1995; Trenberth, 1975, etc). TBO is seen in the rainfall over India (Mooley and Parthasarathy, 1984), and Indonesia (Yasunari and Suppiah, 1988). It is seen in the sea level pressure, sea surface temperature and air temperature in the Indian Ocean region (Terray, 1995). It is also an important component of the El Nino and Southern Oscillation Phenomena (Rasmusson et al., 1990; Roplewski, et al., 1992) and is an integral part of the Asia-Pacific climate. TBO has irregular periodicities ranging from 2 to 3 years. Compared to the stratospheric QBO, it is irregular in period and longitude.

The cause for the TBO is not clearly known. Several theories and hypotheses have been proposed for the cause, development, evolution, southward movement of active convection zone from Indian region to Australia and its interactions with atmosphere – ocean – monsoon systems

and extratropics. Nicholls (1978) postulated that the seasonally varying interaction between the SST in the west equatorial Pacific – maritime continent, and zonal winds in the overlying atmosphere is the cause for TBO. Meehl (1994, 1997) hypothesized that the TBO is due to the coupled ocean- land interactions in the Indian monsoon, Indian Ocean, west and east Pacific regions. The key role played by the land-atmosphere interaction and tropical-midlatitude interactions are also emphasized in his hypothesis. This hypothesis could explain the southward propagation of the TBO signal from Indian summer monsoon region to Australian region well. Tomita and Yasunari (1996) suggested that the northeast winter monsoon plays an important role in the TBO of the ENSO-monsoon system. According to his hypothesis, the SST anomaly in the South China Sea and the winter monsoon maintain the TBO through the tropical-extratropical interactions. A different concept was proposed by Goswami (1995), which attributes to the TBO as a result of pure internal dynamics (boundary conditions such as SST etc do not have any role in its generation). According to his hypothesis the TBO is arising as a result of the modulation of energetic intraseasonal oscillation by annual cycle. Recently Chang and Li (2000) proposed a theory for TBO, which explains most of the features of the TBO reasonably well. They integrated the ideas of air-sea interaction regulated by annual mean state (Nicholls, 1978, Clarke et al., 1998), those involved in ENSO processes and empherical findings derived from observations or models and developed the theory.

In a rather different explanation, TBO is considered as the result of forcing from the QBO in the lower stratosphere through an unknown stratosphere – troposphere interaction (Khandekar, 1996, 1998). Using zonal wind data form Singapore, Korur and Ponape, Yasunari (1989)

suggested that there exists a coherent phase structure between the lower stratospheric zonal wind QBO and biennial scale zonal wind anomalies in the lower and upper troposphere. He showed that the QBO in the lower stratosphere is also coupled with that in the SST anomalies in the equatorial Pacific. He postulated that the stronger than normal convection over Asian monsoon region through the tropical Pacific from northern summer to winter is related to the downward phase shift of QBO in the lower stratosphere in the same seasons, possibly *via* the stronger than normal Kelvin wave energy.

2.2 Total ozone variability

Ever since the pioneering work of Dobson et al., (1929), the variability of column total ozone levels and its association with meteorological processes such as cut-off cyclones (Wirth, 1995), tropopause folds (Baray et al., 2000), tropical cyclones (Baray et al., 1999; Rodgers et al., 1990; Stout and Rodgers, 1992), equatorial deep convective systems (Suhre et al., 1997), QBO (Bowman, 1989; Tung and Yang, 1994 a; 1994 b; Hamilton, 1995; Holton, 1989; Hollandsworth et al., 1995, Ziemke and Stanford, 1994), western disturbances (Mani et al., 1973), Kelvin waves (Ziemke and Stanford, 1994), Rossby-gravity waves (Stanford and Ziemke, 1993), upper and lower stratospheric planetary waves (Wirth, 1993; Hood and Zaff, 1995; Garcia and Hartmann, 1980; Fusco and Salby, 1999), etc has been a subject of fascinating study.

Wirth (1995) presented a mechanistic axisymmetric Eliassen balanced vortex model for the investigation of the role of diabatic heating in the dynamic evolution of a cut-off cyclone and the related stratosphere –

troposphere exchange. Stout and Rodgers (1992) and Rodgers et al., (1990) showed that the upper tropospheric processes that affect the intensity and motion of tropical cyclone also affect the distribution of ozone in a vertical column. They also pointed that the total ozone distribution is not related to the size of the tropical cyclone but the tropical cyclone's intensity. Baray et al., (1999) analysed a case study of spectacular stratosphere – troposphere exchange directly linked to the strong tropical cyclone *Marlene*, which occurred near Mauritius and Reunion Island on April 1995. With this observation they suggested that the mesoscale tropospheric ozone contaminations, which affect the entire tropical free troposphere, could be due to convective effects.

Data from 'Measurement of Ozone by Airbus In-Service Aircraft' (MOZAIC) project revealed the presence of large ozone peaks (100 to 500 ppbv) associated with tropospheric water vapour mixing ratios (0.4 to 0.6 g kg^{-1}) in the troposphere of the equatorial Atlantic Ocean. These airmasses, rich in ozone and humidity, have been associated with the stratosphere to troposphere quasi-isentropic transport by tropical convection (Suhre et al., 1997).

A number of authors have reported the observational evidence for QBO in total ozone in the tropics and extratropics (Angell and Korshover, 1973; Hamilton, 1989). It is clear from these and other studies that atleast in the tropics the ozone QBO is associated with the well-known QBO in temperature and zonal wind. With a simple one-dimensional model, Holton (1989) showed that horizontal advection by the mean Hadley circulation can account for much of the observed meridional asymmetry of the QBO in total ozone. Bowman (1989) used the nine years of total ozone

measurements from TOMS on Nimbus-7 to study the global structure of QBO in total ozone. He found that the interannual variability of total ozone near the equator (10° N to 10° S) is dominated by the QBO. The equatorial ozone anomalies are independent of season and are well correlated ($r > 0.8$) with the equatorial zonal wind. Tung and Yang (1994 a; 1994 b) clarified the observed picture of how the tropical and extratropical manifestations of the ozone QBO are related. In particular, they found that at very low latitudes the interannual ozone variations very closely follow the variations in the prevailing zonal wind, while poleward of ~10° latitude the ozone anomalies seem to depend on the interaction of the dynamical QBO and the annual cycle. They also explained the presence of two prominent peaks in ozone anomaly spectrum in the extratropics; one (near 30 months) corresponding to the dynamical QBO and one (near 20 months) at the expected beat frequencies between the QBO and annual cycle.

Ziemke and Stanford (1994) investigated the Kelvin wave features in total column ozone using version-6 data from TOMS onboard Nimbus-7. Their results showed eastward propagating zonal waves 1-2 with period ~5-15 days, amplitude ~3-5 DU (1-2% of the time mean), and latitudinal symmetry typical of Kelvin waves. Their analyses and model study suggested that the primary source of the perturbations is slow Kelvin waves in the lower to middle stratosphere. In a study with the same data, Stanford and Ziemke (1993) observed Rossby-gravity waves in total ozone. The observed features are episodic, have zonal wavelengths of ~ 6000 km to 10000 km and oscillate with periods of 5-10 days. The modes exhibit westward phase propagation and eastward group velocity.

With a three-dimensional chemical transport model Hadjinicolaou et al., (1997) showed that the interannual variability in midlatitude ozone can be explained only by meteorological variability in the stratosphere. Their model calculated lowest ozone values during 1993 without the representation of Mt. Pinatubo eruption in the model.

Trend in column ozone between 70° S - 70° N from November 1978 to May 1990 were studied by Niu et al., (1992). They found that trend in the TOMS data are highly seasonal and dependent on location. Near the equator, the estimated monthly trends are not significantly different from zero. In high latitudes, most of the estimated monthly trends are negative. Logan (1994) analysed the vertical distribution of trend since about 1970 and discussed the quality of ozonesonde data and inconsistencies among data records. Stratospheric ozone decreases were found from about 24 km to near the tropopause. Tropospheric ozone showed a mixed trend over different parts of the world with variations with time too. Hood and Zaff (1995) attributed longitude dependence of the total ozone trend in January to the decadal changes in the amplitudes and phases of stationary planetary waves. Steinbrecht et al., (2001) reported that linear regression accounting for the QBO, the 11-year solar cycle, stratospheric volcanic aerosol loading and a long-term trend, accounts for 53% of the interannual ozone variance observed in February at Hohenpeissenberg (48° N, 11° E). When tropospheric circulation patterns are added to the regression, they could get a substantially large fraction (81%) of the observed total ozone variance.

Hood and McCormack (1997) investigated the influence of interannual differences in lower stratospheric dynamics on total ozone trends. Chakrabarty et al., (1998) examined the total ozone trends over

Indian subcontinent using Dobson spectrometer data. They computed trend for six Dobson spectrometer stations and compared with TOMS total ozone data. An increasing trend of this species over the years has been noted at all places except at Varanasi. This increase was attributed, partly to the trend of ozone in the troposphere.

Trends in the vertical distribution of ozone are assessed under SPARC project (SPARC, 1998). Recently Staehelin et al., (2001) presented an extensive review of ozone trends. Solomon (1999) reviewed all aspects of Polar ozone depletion processes in a very detailed way. A number of key problems in atmospheric chemistry are shaped by the strength and character of the various mechanisms acting to move and mix air in the upper troposphere also. Mahlman (1997) examined the transport process from a mechanistic perspective, with primary emphasis on the tropopause and middle-troposphere regions in the extratropics.

Chapter –3

Data and Methodology

3.1. General

Monthly mean radiosonde data over Thumba, Trivandrum, daily and monthly reanalysis data sets from National Centers for Environmental Prediction / National Center for Atmospheric Research (NCEP/NCAR), total ozone measured by TOMS instrument onboard Nimbus-7, Indian summer monsoon rainfall data (Parthasarathy et al., 1994), details of break periods in Indian summer monsoon activity from De et al., (1998) are mainly used in the thesis.

3.2 High-resolution radiosonde data over Thumba, Trivandrum

An Indian radiosonde system working on 1680 MHZ, measuring temperature and wind more or less regularly on weekly basis at Thumba is used in this work. An erstwhile USSR made radiosonde system working on 1780 MHZ is also employed. The course of hydrogen filled balloon release with radiosonde system and corner reflector is tracked by radar and telemetry system and the meteorological parameters, azimuth, elevation and range at 1 minute interval are recorded at the ground.

The accuracy of the wind measurement is 1 ms^{-1} and probable mean square error of temperature is less than 0.4° C, from 40° C to -90° C. The monthly values in the altitude range 0-30 km for a period of 23 years, extending from January 1970 to December 1992, constituted the basis data for this work. The numbers of observations above 30 km being less, data above 30 km were not used for the analysis. The weekly values of wind and temperature

were averaged over a period of each month to obtain the monthly mean values at every 1 km altitude intervals.

3.3 NCEP/NCAR reanalysis data

In chapters 5 and 6, 40-year (1957-96) global NCEP/NCAR reanalysis data set is used to study the circulation of the atmosphere. Reanalysis contrast the 'traditional' data sets in two fundamental ways: (1) an atmospheric general circulation model (AGCM) is an integral component of the analysis system and (2) a wide range of observations are used. Thus, reanalysis not only provides potentially very useful dynamical quantities that cannot be determined by subjective analysis, but may be more accurate than such traditional analyses, particularly in data sparse regions. However, the differences in the AGCMs and the analysis methods will lead to differences in reanalysis. Several inter comparison studies have been made to understand the magnitude and nature of this uncertainty in NCEP/NCAR reanalysis.

The NCEP assimilation system used observations from the COADS surface marine dataset, the rawinsonde network, satellite soundings (the Tiros Operational Vertical Sounder, TOVS data), aircraft data, and satellite (GMS, GOES, and METEOSAT) cloud drift winds. These data were subject to stringent quality control (Kalnay et al., 1996). To interpolate the data into model grid, a spectral statistical interpolation (SSI) was used; this is a three dimensional variational technique. A T62 global spectral model, corresponding to approximate grid point spacing of 208 km was used in NCEP reanalysis. This model used σ-levels as vertical co-ordinate.

The reanalyzed gridded fields have been classified into four classes, depending upon the relative influence of the observational data and the model on the gridded variable (Table 3.1).

Reanalysis outputs are available in 17 standard pressure levels (hPa), 11 isentropic surfaces (K) and 28 sigma levels. The horizontal resolution is 2.5° longitude × 2.5° latitude.

Class	Relative Influence of Observational Data and Model on Reanalysis Variable
A	Strongly influenced by observational data *(most reliable)* *[e.g. upper air temperature and wind]*
B	Model has very strong influence than observational data *[e.g. humidity and surface temperature]*
C	Derived solely from model fields forced by data assimilation to remain close to the atmosphere. *[e.g. clouds, precipitation, and surface fluxes]*
D	Obtained from climatological values and does not depend on model *[e.g. plant resistance, land-sea mask]*

Table 3.1. Classification of NCEP/NCAR reanalyzed fields.

Standard pressure levels (hPa) are 1000, 925, 850, 700, 600, 500, 400, 300, 250, 200, 150, 100, 70, 50, 30, 20, and 10.

Isentropic surfaces (K) are 650, 550, 450, 400, 350, 330, 315, 300, 290, 280 and 270.

Sigma levels are 0.9950, 0.9821, 0.9644, 0.9425, 0.9159, 0.8838, 0.8458, 0.8014, 0.7508, 0.6943, 0.6329, 0.5681, 0.5017, 0.4357, 0.3720, 0.3125, 0.2582, 0.2101, 0.1682, 0.1326, 0.1028, 0.0782, 0.0580, 0.0418, 0.0288, 0.0183, 0.0101, and 0.0027.

NCEP/NCAR reanalysis data have good vertical coverage in the stratosphere also. There are 7 pressure levels and 4 isentropic surfaces present above the tropical tropopause. NCEP/NCAR data set has been validated with observational data sets. In a series of studies (Pawson and Fiorino, 1998a; 1998b; 1999) validated the tropical stratosphere (thermal structure, annual cycle, QBO etc) in NCEP data. They found good agreement between observed values and reanalysis values. At the uppermost level (10 hPa), the reanalysis system found to perform poor due to the proximity of the upper boundary.

3.4 All India summer monsoon rainfall series

Several Indian summer monsoon rainfall series have been prepared with the number of rainguages varying from 300 to 3000 spread all over India for the different lengths of period starting from the year 1841 onwards. But the most systematic rainfall series was prepared by Parthasarathy et al., (1994)

based on fixed network of rainguages. This series is available for the period 1871 to 1993, based on 306 well-distributed rainguage stations over India, one from each of the districts in the plain region (29 subdivisions) of India. The monthly rainfall data at these 306 stations were taken from the records of the India Meteorological Department. Proper weightage for each rainguage station assigning the district area as the weight was given while preparing the rainfall series. The all India summer monsoon rainfall series is presented in fig 3.1.The mean all Indian summer monsoon rainfall (June to September) is 852.4 mm with a standard deviation of 84.69 mm.

3.5 Breaks in Indian summer monsoon activity

Indian summer monsoon activity is characterized by active and break cycles. The India Meteorological Department defines a 'break in the monsoon' as a general cessation of precipitation over most of India with exception of the very south of Peninsular India and the foothills of Himalayas. This rainfall pattern is accompanied by a rise in surface pressure of 2-3 hPa over central India as the monsoon trough moves northward. Enhancements of rainfall and monsoon flow in between the breaks are called as 'active period in the monsoon'. De et al., (1998) identified the break periods during the 30-years (1968-97).

Magana and Webster (1996) argued that the break and active periods in monsoon flow are on a scale much larger than India or even south Asia. They suggested a criterion (see table 3.2) to define active and break periods during

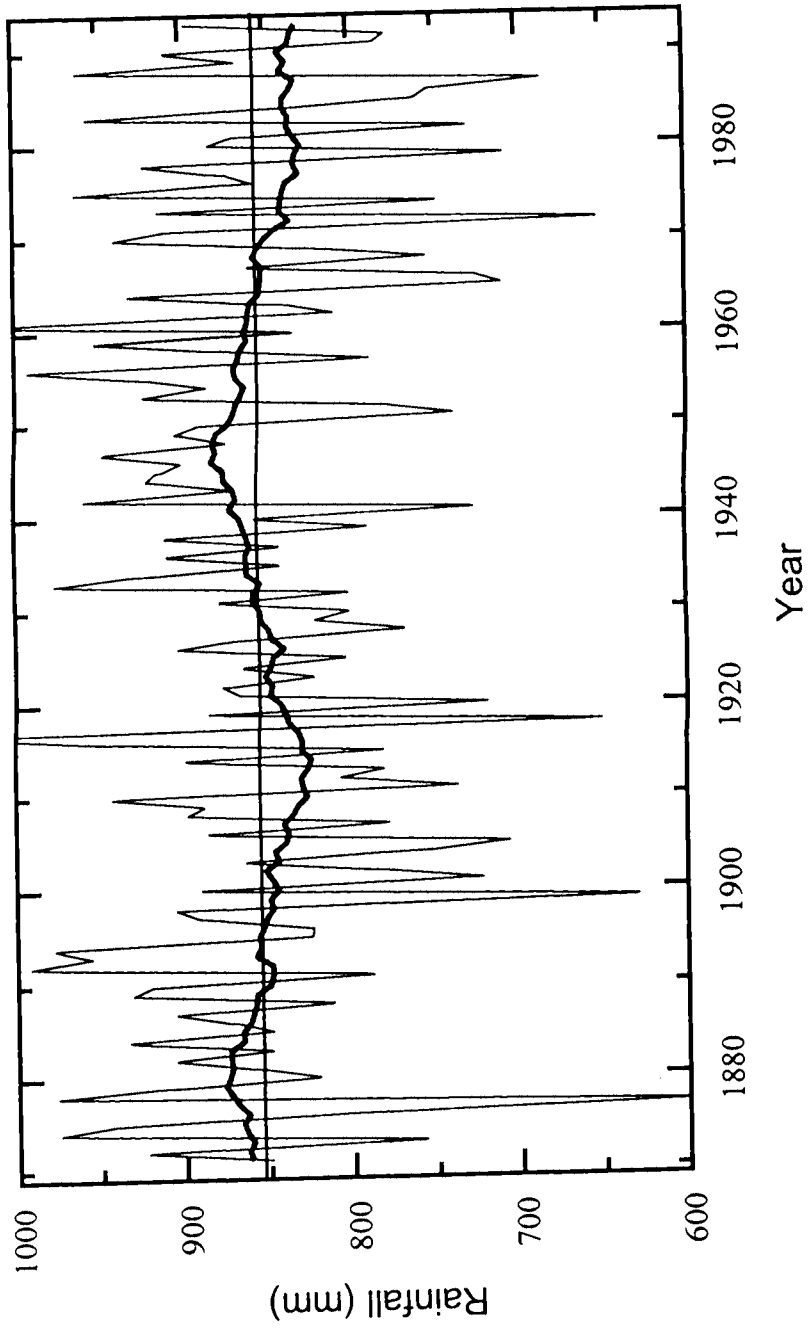

Fig. 3.1 All India summer monsoon rainfall in mm. Thick line is the 31 year adjacent average.(Data from Parthasarathy et al, 1994)

the boreal summer Asian-Australian monsoon and the active/break periods during 1980-93 was tabulated by Webster et al., (1998).

Condition	**Active** (Anomaly)	**Break** (Anomaly)
850 hPa meridional wind at (45° E, 0° N), ms^{-1}	>3	>-3
850 hPa zonal wind at (65°- 95° E, 10°- 20° N), ms^{-1}	>3	>-3
Outgoing longwave radiation at (65°- 95° E, 10°- 20° N), W m^{-2}	<10	>10

Table 3.2 Criteria used to define active and break periods of boreal summer monsoon (After Magana and Webster, 1996)

3.6 Global total ozone data

The TOMS instrument onboard Nimbus-7 provided the global coverage of total ozone on daily basis. The Nimbus 7 spacecraft was in a south-to-north, sun-synchronous polar orbit so that it was always close to local noon/midnight below the spacecraft. Thus, ozone measurements were taken for the entire world every 24 hours. TOMS directly measures the backscattered ultraviolet sunlight from the earth's atmosphere. Total ozone is derived from the differential absorption of scattered sunlight in the ultraviolet region. Ozone is

calculated by taking the ratio of two wavelengths (312 nm and 331 nm, for example), where one wavelength is strongly absorbed by ozone while the other is absorbed only weakly. The instrument has a 50 km square field of view at the sub-satellite point. TOMS collects 35 measurements every 8 seconds as it scans right to left producing approximately 200,000 ozone measurements daily. These individual measurements vary typically between 100 and 650 Dobson Units (DU) and average about 300 DU. This is equivalent to a 3 mm thick layer of pure ozone gas at STP conditions.

Although the total ozone data obtained from TOMS instrument are available from Nimbus-7, Meteor-3 and Earth Probe satellites, the data obtained from TOMS onboard Nimbus-7 are used in this study. This data set is continuous, regular and available for a relatively long period (14.5 years, 31 October 1978 – 6 May 1993).

The TOMS data [version-7] (Mc Peters et al., 1996) are available as (a) gridded daily, (b) gridded monthly average, (c) GIF image, (d) overpass data and (e) zonal means. These data are available in the form of CD-ROMS. Also TOMS data is available in Goddard Space Flight Laboratory's (USA) website *(http://toms.gsfc.nasa.gov)*. TOMS (Nimbus-7) data are available for the period 31 October 1978 – 6 May 1993 (~14.5 years).

(a) Gridded daily

Daily TOMS measurements have been arranged in to 1.25° lon × 1.0° lat grids from 90° S to 90° N and 180° W to 180° E longitude. Thus the

gridded dataset has 180x288 ASCII data arrays. Each total ozone value is in 3-digit integer format. Also local equatorial crossing time is also provided in the data set.

(b) Gridded monthly avergae

The gridded monthly average data also have the same format as gridded daily data. Average over a cell is made only when good quality data was available for the cell at least for 20 days.

(c) GIF image

Each day of data has a corresponding GIF image with 640×480 pixels (full screen in standard VGA) at 256 colours. Images are available in polar (south and north) and Aitoff projections.

(d) Overpass data

Best matching single observation for 371-ground locations worldwide is provided in this data.

(e) Zonal means

Daily and monthly zonal averages in 5° latitude zones are provided in this data.

3.6.1 Comparison of TOMS data with ground-based total ozone measurements

The TOMS version-7 data have been compared with ground based measurements made by a network composed of 30 mid-northern latitude stations with Dobson and Brewer ozone measuring instruments. Only stations had homogeneous data coverage for the entire 14.5 year lifetime of TOMS instrument were included for comparison study. A weekly mean was computed from the daily TOMS-ground differences at each station. These differences from the 30 stations were then averaged to derive a weekly average TOMS-ground difference. In fig. 3.2, the percentage difference between TOMS and ground based ozone measurements as a function of time is presented (from Mc Peters et al., 1996). The difference is smaller than the combined uncertainty of the TOMS and ground based measurements and of the comparison technique, as is the overall trend of 0.2 percent/decade. Thus the two methods of total ozone measurements agree to within the uncertainties.

3.6.2 Problems with the TOMS version-7 data

Volcanic eruptions, solar eclipses, polar stratospheric clouds, high terrain, etc affect the total ozone measured by TOMS instrument. Problems were noticed after the eruptions of El Chichon in April 1982 and Mt. Pinatubo on June 15, 1991. Gaseous SO_2 erupted from these major eruptions absorbed the bands in 290 nm to 320 nm range. Some bands at longer wavelengths coincide with wavelengths used by TOMS to measure total ozone. This produced a false enhancement of total ozone measured by TOMS. This

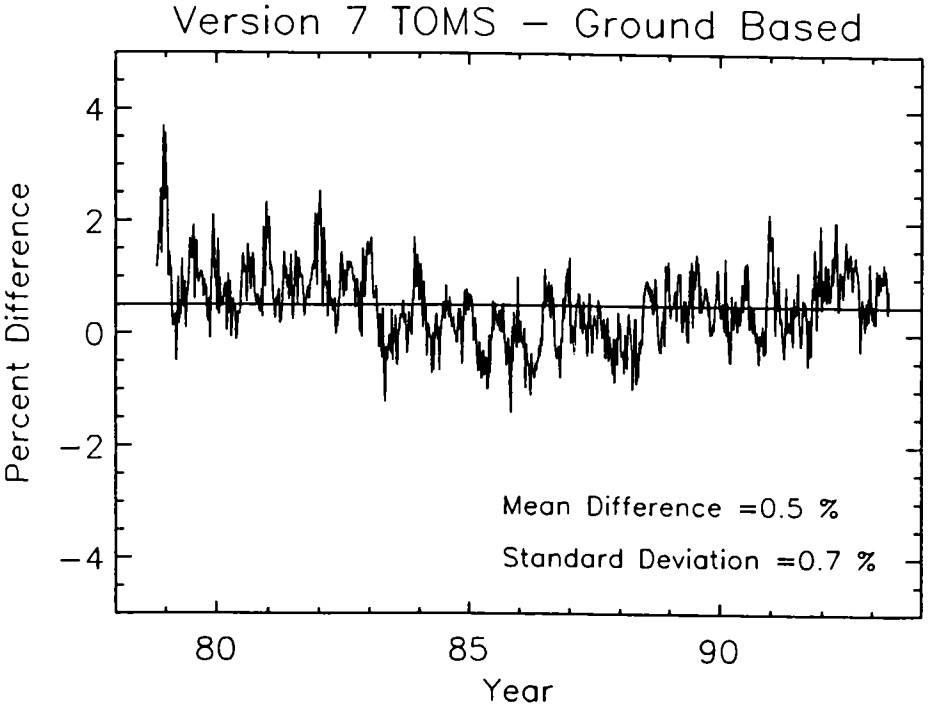

Fig. 3.2 Percentage difference between TOMS and ground ozone. Solid line is linear fit trend. (After McPeters et al, 1996).

problem is short-lived because the SO_2 is converted rapidly to sulfuric acid aerosols. The contaminated data points were marked with a flags for identification.

TOMS measures backscattered sunlight for total ozone estimation. It is not possible to measure ozone when there is no sun. Because of this reason, total ozone data are missing for polar winter season. Another feature observed in TOMS measurements were the low ozone values present over high mountain regions. Because of high terrain, the column of ozone is lower over these regions. This is not an error. TOMS measurements suffered another problem due to the solar eclipses. The decrease in incoming solar radiation leads to a decrease in backscattered radiance. So ozone values were not retrieved for periods of time and ranges of latitude where the radiances are affected by a solar eclipse.

3.7 Wavelet analysis

Wavelet transform is an analysis tool well suited to study multi-scale, non-stationary processes occurring over finite spatial and temporal domain. Since its introduction by Morlet (1983) over a decade ago, this technique has found wide application in diverse fields. The wavelet transforms can be used to analyze time series that contain non-stationary power at many different frequencies. Wavelet analysis gives the localized variations of power within a time scale, by decomposing a time series in time- frequency space and one is able to determine both the dominant modes of variability and how those mode vary in time.

3.7.1 Wavelet transforms

The Wavelet Transform (WT) is a generalized form of Fourier Transform (FT) and a Windowed Fourier Transform (WFT), (Gabor, 1946). The FT uses sine and cosine functions that have infinite span and are globally uniform in time. The FT does not contain any time dependence of the signal and therefore cannot provide any local information regarding the time evolution of its spectral characteristics. In WFT, a time series is examined under a fixed time-frequency window with constant intervals in the time and frequency domains, and hence over-represents high-frequency components and under-represents low-frequency components.

A WT uses generalized local base functions (wavelets) that can be stretched and translated with a flexible resolution in both frequency and time. The flexible windows are adaptive to the entire time-frequency domain, known as the wavelet domain (WD), which narrows while focusing on high-frequency signals and widens while searching the low-frequency background. As a result, high precision in time localization in the high-frequency band can be achieved at the reduced frequency resolution, and vice-versa for low frequency components. A wavelet transform allows the wavelets to be scaled to match most of the high-and low-frequency signals so as to achieve the optimal resolution with the least number of base functions. This Zoom-in property is very unique of the WT that allows the localization of very short-lived, high frequency signals in time, such as abrupt changes, while resolving the low-frequency variability in the time scale or frequency more accurately with relative ease in computation.

Mathematically, a WT decomposes signal s(t) in terms of some elementary functions $\psi_{b,a}(t)$ derived from a Mother Wavelet or analyzing wavelet $\psi(t)$ by dilation and translation:

$$\psi_{b,a}(t) = 1/(a)^{1/2} \quad \psi(t-b/a) \qquad ...(3.1)$$

where b denotes the position (translation) and a(>0) the scale (dilation) of the wavelet, $\psi_{b,a}(t)$ are called daughter wavelets or simply wavelets. An energy normalization factor $(a)^{-1/2}$ keeps the energy of the daughter wavelets the same as the energy of the mother wavelet.

3.7.2 Graphical representation

The choice of octave which is logarithmic with the base of 2 for the frequency or time scale, as a unit to divide the frequency domain allows us to include a broad range of scales, from very small to very large, in an efficient way in a coordinate system with linear interval in octave while logarithmic in frequency scale. In a continuous WT where more scale decomposition is desired, each octave may be divided further by infinite voices. Thus unlike the FT that maps a 1-D time series to a 1-D spectrum, the WT maps a 1-D time series to a 2-D image that portrays the evolution of scales and frequencies with time.

3.7.3 Wavelet choice

There are many commonly used analyzing wavelets that can be grouped into two main categories; continuous wavelets and orthogonal wavelets (a discrete wavelet transform may not be orthogonal.) One of the most widely wavelets in geophysics is the complex Morlet Wavelet, which consists of a plane wave modified by a Guassian envelope. Another commonly used continuous wavelet is the Mexican Hat, which is the second derivative of the Guassian Function. The simplest orthogonal wavelet is the Harr wavelet, which is based on a Box function. In our analysis we have used the Morlet Wavelet whose function.